

Journal of Nanophotonics

SPIEDigitalLibrary.org/jnp

Microspot sensing based on surface-enhanced fluorescence from nanosculptured thin films

Alina Karabchevsky
Chinmay Khare
Bernd Rauschenbach
Ibrahim Abdulhalim



Microspot sensing based on surface-enhanced fluorescence from nanosculptured thin films

Alina Karabchevsky,^a Chinmay Khare,^b Bernd Rauschenbach,^b and Ibrahim Abdulhalim^a

^aBen-Gurion University of the Negev, Department of Electrooptic Engineering and Ilse Katz Institute for NanoScale Science and Technology, Beer-Sheva 84105, Israel

rudenko@bgu.ac.il

^bLeibniz-Institut für Oberflächenmodifizierung e.V., Permoserstrasse 15, 04318 Leipzig, Germany

Abstract. Nanosculptured thin films (STF) are prepared by the oblique angle deposition technique and take different forms of nano columnar structures. Varieties of STFs were investigated to find the optimum structure for biosensing based on the surface enhanced fluorescence. A comparative study was carried out with STFs containing the nanocolumnar structures that differ in their shape, height (h), and tilt angle with respect to the surface (α), thickness (d), and arrangement. The greatest enhancement of the fluorescent signal was found for Ag-based STFs on Si (100), giving an enhancement factor of $\times 71$, where $h = 400$ nm, $d = 75$ nm, and $\alpha = 23^\circ$ relative to Ag closed film using fluorescent dye Rhodamine 123. We immobilized the fluorescent receptor to the thiol self-assembly monolayer on Ag-based STF and Ag dense film to demonstrate the applications of STFs for specific biosensing. Upon excitation of the fluorophore by an Hg light source, a CCD camera with controlled exposure time would detect the pattern of fluorescent receptor Anti-Rabbit IgG on the surfaces. A specially designed optical fiber housing attached to the microscope allowed quantitative measurement of the fluorescence spectrum on a microspot parallel to the image grab. © 2012 Society of Photo-Optical Instrumentation Engineers (SPIE). [DOI: [10.1117/1.JNP.6.011508](https://doi.org/10.1117/1.JNP.6.011508)]

Keywords: optical biosensing; sculptured thin films; fluorescence spectroscopy; surface enhanced fluorescence.

Paper 11122SS received Nov. 24, 2011; revised manuscript received May 1, 2012; accepted for publication May 3, 2012; published online Jun. 21, 2012.

1 Introduction

The quest for optical methods capable of detecting trace amounts of biologically important molecules under physiological conditions can be traced back to Hirschfeld, who demonstrated in the mid-1970s detection of a single antibody molecule tagged with 80 to 100 fluorophores.¹ Planar integrated arrays of sensors based on using a mature technology, such as the Si technology² has great advantage for biochips.³ Fluorescence is one optical phenomena that can be used to detect biopathogens on surfaces; however, fluorescent emission from analytes, especially from biological assays, is weak. In order to increase the fluorescent signal from an analyte, attempts have been made to increase the number of dye molecules bound to the surface, but this produces concentration quenching, reducing first the quantum efficiency and then the total emission. Surface enhancement and therefore fluorescence can be achieved due to special morphology of the metal nanosculptured surfaces. It is widely accepted that the mechanism for surface-enhanced processes is predominantly electromagnetic in nature. Metal nanoparticles and nanostructured metal films possess localized surface plasmon resonances (LSPRs) that imbue these materials with a number of unique and useful optical properties.⁴ Clear evidence for the role of local plasmon resonances in the excitation and emission processes has been presented.⁵ LSPRs are responsible for the size- and shape-dependent optical spectra leading to the use of metal

nanoparticles in a variety of bio-diagnostic applications⁶⁻⁸ and plasmon modes have been implicated in the extraordinary transmission of light through nanoscale hole⁹ and slit¹⁰ arrays. Furthermore, the confined local electric field enhancements that accompany the excitation of LSPRs are used in a variety of near-field enhanced spectroscopy and imaging modes, from near-field scanning optical microscopy^{11,12} to surface-enhanced Raman spectroscopy (SERS).¹³⁻¹⁸ Although SERS applications have motivated much of the research into surface-enhanced spectroscopy in the past decade, the widespread use of fluorescence-based sensing in biology and the importance of radiative decay near metal electrodes in organic optoelectronics^{19,20} are two factors leading to new interest in the study of simple fluorescence near metal nanostructures.²¹ Although planar metal films generally quench the emission from nearby fluorophores,^{22,23} the effects of metal nanostructures are more complicated. Depending on the details of the system under investigation, fluorescence quenching,²⁴⁻²⁶ enhancement,^{5,27-30} or both³¹ have been reported in experimental studies of fluorescent dyes and quantum dots near nanostructured metals.

The increased surface area (and hence the increased quantity of adsorbed dye) of a nanostructured metal surface compared with a planar substrate or dens film might account for some of the reports of enhancement. The observation of enhancement in single molecule experiments,^{5,26} planar dye layers with adsorbed nanoparticles,²⁷ and the observation of fluorescence signal amplification due to the sculptured thin films (STF)³² indicate that real, nontrivial enhancements of fluorescence using near-field effects are achievable. The origins of such nontrivial fluorescence enhancement effects near nanostructured metal can be understood as arising from two contributions. First, by concentrating the incident light into local nanoantennas, nanostructured surfaces can lead to increased absorption of the incident light by the fluorophores. Second, metal nanostructures can alter the radiative and the nonradiative decay rates of nearby fluorophores, changing both the fluorescence lifetime and quantum yield. Although it has remained difficult to separate the effects of excitation and emission enhancement, both of these local field effects are expected to be extremely sensitive functions of the shape of the metal particle, the orientation of the dye, and the distance between the dye and the metal,^{33,34} just as they are for dyes attached to planar metal films.^{22,23} In this paper we present an extensive comparative study of enhanced fluorescence from a variety of nanometallic thin films versus dens films on different substrates. The main purpose of this study is to demonstrate biosensing from the microspot area based on the amplification of fluorescence signal due to the special surface morphology of STF.

STFs^{35,36} are nanostructured materials with unidirectionally varying properties that can be designed and realized in a controllable manner using variants of physical vapor deposition techniques. The growth mechanism is based on self-organized nucleation during deposition and subsequent highly directional growth due to an atomic shadowing mechanism. A particle flux, incident to the substrate at an angle a (usually $a \geq 80$ deg, as measured with respect to the substrate normal), enables preparation of columnar thin films under oblique angle deposition.³⁶ The ability to instantaneously change the growth direction of their columnar morphology, through simple variations in the direction of the incident vapor flux, leads to a broad spectrum of columnar forms such as spiral, screws, vertical columns, and chevrons. To date, the chief applications of STFs are in optics as polarization filters, Bragg filters, and spectral hole filters.^{37,38} At visible and infrared wavelengths, a single-section STF is a unidirectionally non-homogeneous continuum with direction-dependent properties. Being porous, an STF can act as a sensor for fluids. Recent experimental results³⁹ and theoretical SPR calculations^{40,41} show a great potential for using STFs as SPR sensors. Biomedical applications such as tissue scaffolds, drug-delivery platforms, virus traps, and lab-on-a-chip are also in different stages of development.^{42,43} STF are new potential materials for fluorescent enhancement near the surface.⁴⁴ In this work we present an extensive study towards biosensing based on a surface-enhanced fluorescence phenomenon from nanostructured metal STFs. A broad comparative study was done using Rhodamine 123 as a fluorophore on a variety of films that differ by their morphology, materials as metals and substrates, inclination angles, height (h), tilt angle with respect to the surface (α), thickness (d), and arrangement to find the best STF candidate for biosensing applications. We used: (1) Rhodamine 123 as a fluorescent dye to stain the special surfaces of STFs. After the staining by Rhodamine 123 we compared different STFs and their references to show the amplification of fluorescent signal due to the metal nanosculptured surfaces. The samples were quantified by means of the fluorescent signal from captured fluorescence images and

fluorescence spectra using a spectrometer. A special optical fiber holder was designed and inserted into the microscope in place of the eyepiece and guided the fluorescence signal to the spectrometer. By immobilizing the fluorescent antibody to the thiol self-assembly monolayer on surfaces we show the applications of the STF as a specific biosensor.

2 Experimental

2.1 Preparation of STFs

STFs were prepared using the oblique angle deposition technique.⁴⁵ STFs of different materials, such as Si, Ag, Au, and Cu on different substrates, were prepared by methods including sputter deposition and e-beam evaporation. The deposition angle was adjusted to $a = 85$ deg (deposition angle a as measured with respect to the substrate normal) to form nanostructures of manifold shapes (spirals, screws, vertical columns)³⁶ using appropriate substrate rotation schemes. Subsequently, dense films of each material were also deposited with deposition angle $a = 0$ deg, as reference samples. Pre-patterned substrates, comprising monolayers of SiO₂ nanospheres prepared by a self-assembly⁴⁶ method, and Au dot honeycomb-like array gained by evaporating Au through the voids of such self-assembled nanospheres,⁴⁷ were used to form periodic nanostructure arrays.

The Si, Cu, and Ag STFs were grown by ion-beam sputter oblique angle deposition,^{48–50} the Au nanorod STFs were grown with direct current (dc) sputter oblique angle deposition, and the Ag nanorod STFs by means of electron-beam-evaporation oblique angle deposition³² [Fig. 1(a)]. The deposition of Ag and Au films was carried out in a combined electron-beam evaporation and sputtering system (Edwards). The distance between the source and the substrate was kept at approximately 16 cm for electron-beam evaporation, with the nominal deposition rates measured with a resonating quartz crystal sensor. Ion beam sputter oblique angle deposition (for Si, Cu, and Ag nanostructures) was carried out in a high vacuum deposition chamber with a base pressure of 1.0×10^{-6} Pa as described elsewhere.^{48,50} A sintered target (purity 99.999%) was sputtered by a 1000 eV Ar⁺-ion beam, extracted from a radio-frequency (13.56 MHz) ion source with a triple-grid ion extraction system (grid diameter 40 mm). Argon gas with a mass flow of $f_{Ar} = 5.50$ sccm as a process gas, was kept constant for all experiments. After growth, the topography

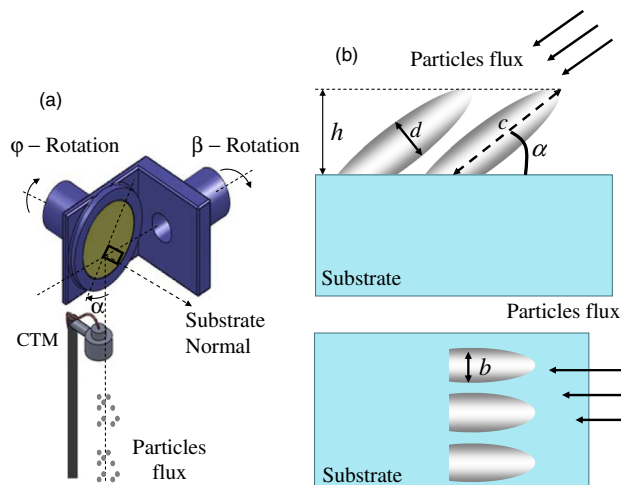


Fig. 1 (a) Schematic of the oblique angle deposition setup. One stepper motor controls deposition angle β , and a second stepper motor is used for substrate rotation φ about the substrate normal. CTM = crystal-thickness monitor, PVD = physical vapor deposition. (b) Illustration of the columns' creation during the evaporating process: side view with h vertical height, d is rods' transverse diameter (along the major axes) in the plane of incoming vapor flux, α is the inclination angle normal to the substrate, and the top view with b the rod conjugate diameter (along the minor axes) perpendicular to the plane of incoming vapor flux. Note that the inclination angle α shown in (b) is actually determined by the tilt angle of the substrate shown in (a).

of the samples was examined with scanning electron microscopy (SEM) at 2.5 kV acceleration voltages. Analysis of the SEM micrographs was done using a commercially available Scanning Probe Image Processor (version 3.2.6.0.) with the grain detection module. A schematic illustration for the oblique angle deposition setup and the general structure of the rods is demonstrated in Fig. 1(a) and 1(b), respectively. A wide variety of STFs were prepared by the above methods. Among these STFs are silicon spirals on SiO₂ nanospheres, silicon spirals on gold dots, silicon rods on polystyrene nanospheres, Cu nanorods with various heights on silicon and fused silica (f.s.) substrates, Ag nanorods, and Au nanorods on silicon and f.s. substrates.

2.2 Preparation of Fluorescent Dye

For fluorescence measurements, the samples were spin-coated at 4000 RPM with fluorescent dye Rhodamine 123 diluted in methanol at 0.6 wt%. The thickness of the spun dye layer was estimated by atomic force microscope measurements to be approximately 50 nm. Care was taken in selecting the spinning conditions to obtain uniform dye films and similar thicknesses on both the sample and its reference.

2.3 Fluorescence Microscopy Imaging

With light microscope optics adjusted for fluorescence microscopy, it is possible to examine the distribution of a single molecular species in a specimen and, under specialized conditions, even detect individual fluorescent molecules. In contrast to other forms of light microscopy based on object-dependent properties of light absorption, optical path differences, phase gradients, and birefringence, fluorescence microscopy allows visualization of specific molecules that fluoresce in the presence of the excitation light source.⁵¹ In this study, fluorescence measurements were performed using an Olympus fluorescence upright microscope BX51 with an Hg arc lamp as excitation light source. The green Hg line at 546 nm was used for excitation in all of the experiments and the emission was detected using the red filter at 590 nm.

Light passing through the objective lens propagates as a parallel beam, which is collected by an internal tube lens as an aberration-free image in the real intermediate image plane (Fig. 2). Detection of the image/signal obtained in the intermediate image plane was performed: (1) using a high sensitivity cooled CCD camera with a controlled exposure time, the acquired images were then analyzed using Matlab and the average intensities of the sample and its reference were compared; and (2) the measurements were also performed using a fluorescence spectrometer. The light from the mercury lamp was focused on the analyte samples (dye or fluorescent receptor) by Olympus semi-apochromatic UIS2 objectives lenses $\times 20$ and $\times 50$ MPlanFLN, infinity corrected (with 0.45 and 0.8 numerical apertures, respectively). The presented measurement was

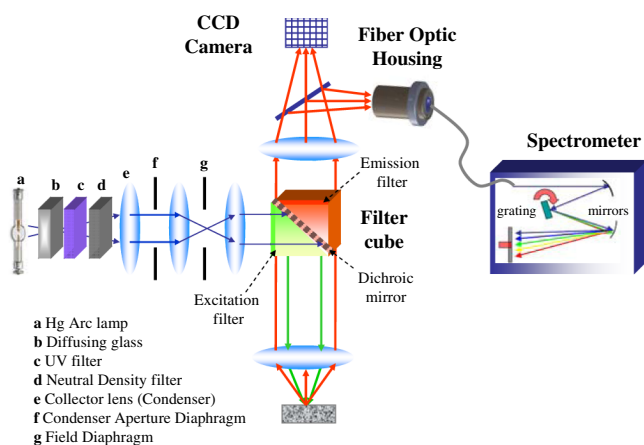


Fig. 2 Schematic drawing of the optical setup utilizing LSPR-enhanced fluorescence spectroscopy collecting the signal through the fiber optic at the intermediate plane of the fluorescent microscope.

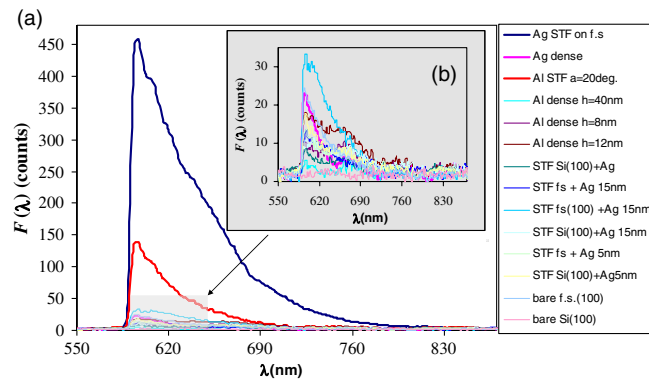


Fig. 3 (a) Fluorescence spectra obtained using the microspectrofluorometer from some of the samples covered by Rhodamine 123 used in the study for 10 ms exposure time with $\times 50$ objective; (b) Zoom on the low intensity signals.

performed for $30 \times 30 \mu\text{m}$ areas with 300×300 pixel resolution and total acquisition time of 3 s. Matlab software was used to analyze the data.

2.4 Microspot Spectral Fluorometry

Due to the integration of the microscope with a spectrometer, the fluorescence emission spectrum was recorded simultaneously with the image grab. We designed a special optical fiber holder to fit in place of the standard microscopic eyepiece (Fig. 2) with possible XY and focus adjustments. The distal end of the fiber is connected to the spectrometer and the strongest signal is obtained when the fiber is placed in the plane of the primary image of the microscope.

The acquired spectra were filtered from noise by a median filtering technique using Matlab and then analyzed (Fig. 3). The maximal values of the sample and its reference were compared to obtain the fluorescence emission enhancement factor ($e.f.$). The microspot diameter, D_{spot} , being inspected is determined by the microscope's primary magnification M and the diameter of the fiber D_{fiber} ($D_{\text{spot}} = D_{\text{fiber}}/M$). Hence in our case using $D_{\text{fiber}} = 1 \text{ mm}$ and $M = 50$, the spot diameter is $D_{\text{spot}} = 20 \mu\text{m}$. The background was removed from the received spectra using Matlab software. Micro spot fluorometry enabled investigation of the effects of amplification of the fluorescent signal from STFs and reference films in a more quantitative fashion. Size of the microspot defines the dimensions of the sample being detected quantitatively with the spectrometer and smaller spot allows detecting smaller bioentities such as single cells.

3 Results and Discussion

3.1 Fluorescence Signal from a Variety of STFS Using Rhodamine 123

For each sample, a substrate or a dens film of the same material and with the same thickness deposited on a similar substrate was taken as a reference. The enhancement factor is defined as the ratio between the fluorescence signal of the STF $F(\lambda)_{\text{STF}}$ and the fluorescence signal from the corresponding reference film $F(\lambda)_{\text{ref}}$ after the background subtraction:

$$e.f. = \frac{F(\lambda)_{\text{STF}}}{F(\lambda)_{\text{ref}}} \quad (1)$$

Fluorescent signals $F(\lambda)$ were achieved by reducing the background: $F(\lambda) = F(\lambda) - \min\{F(\lambda)\}$. Some of the $e.f.$ values were calculated according to the fluorescence images. In our pioneering work on surface enhanced fluorescence (SEF) from STF in which *Escherichia coli* bacteria detection was demonstrated, we reported^{32,52} on $e.f.$ of 15 or larger with respect to glass substrates. Furthermore, if we subtract the background from the fluorescence peak values reported in^{32,52} and then calculate the ratio, an enhancement factor of 20 instead of 15 is obtained

Table 1 Summary of the nano-STF used in the study and their fluorescence *e.f.*

| # | Sample | Enhancement | Reference | Description |
|----|--|-------------------------|--------------------------|--|
| 1 | Ag STF nanorods (4 samples) | 23*, 20** | *Ag closed film, **f.s. | $h = 400$ nm, $d = 75$ nm, $\alpha = 23^\circ$, on f.s. substrate |
| 2 | Al STF nanorods | 36.66*, 5.9,** | *Al dense, **f.s. | $h = 1000$ nm, $d = 30$ nm, $\alpha = 20^\circ$, on f.s. substrate |
| 3 | Si STF with evaporated top layer of Ag on Si (2 samples) | 9.6*, 2.15** | *Ag dense, **Si | Si rods ($h = 50$ nm or 100 nm), $\alpha = 90^\circ$, on Si substrate and Ag nanolayer (5 nm and 15 nm) on top |
| 4 | Cu STF nanorods | 2*, (1-3)** | *Cu dense, **Si and f.s. | Cu nanorods 220 nm height on Si substrate, $\alpha = 90^\circ$ or Cu nanorods 550 nm height on silica substrate, $\alpha = 90^\circ$ |
| 5 | Ag islands (4 samples) | 4 ± 1 | Si and f.s. | 5 nm and 15 nm thick islands of Ag on Si and f.s. substrates |
| 6 | Si STF with evaporated top layer of Ag on fused silica substrate (2 samples) | 0.5 | f.s. | Si rods ($h = 50$ nm or 100 nm), $\alpha = 90^\circ$, on f.s. substrate and Ag nanolayer (5 nm and 15 nm) on top |
| 7 | Si spirals on Au nanodots | 0.58 | Si | Si spirals, $h = 740$ nm, grown on honeycomb like Au nanodots of 30 nm height patterned on Si substrate |
| 8 | Si-STF (4 samples) | 0.22–3.46 | Si or Glass | Si rods, $h = 50$ – 100 nm on Si or glass substrates, $\alpha = 90^\circ$ |
| 9 | Cu-STF (4 samples) | ~2.20 | f.s. | $h = 45$ – 100 nm, $d = 30$ – 60 nm, $\alpha = 20^\circ$, on f.s. |
| 10 | Cu-STF (4 samples) | (0.8–1.2)*, (0.1–0.3)** | *Cu dense, **f.s. | $h = 100$ – 1100 nm, $d = 40$ – 150 nm, $\alpha = 30$ – 42° , on f.s. substrate |
| 11 | Si spirals on SiO ₂ nanospheres | 0.61 | Si | $h = 1090$ nm, Si substrate templated with mono-layer of SiO ₂ nanospheres (diameter 350 nm) |
| 12 | Au STF nanorods | 3.85*, 0.85** | *Au dense, **f.s. | $h = 285$ nm, $d = 40$ nm, $\alpha = 35^\circ$, on f.s. substrate |
| 13 | Ag STF nanorods | 51.5*, 26.4** | *Ag dense, **Si(100) | Ag nanorods height 170 nm (the first 70 nm is closed) without capping layer on Si(100) |
| 14 | Ag STF nanorods | 10*, 5.15** | *Ag dense, **f.s. | Ag nanorods height 170 nm (the first 70 nm is closed) (nominal) 10 nm Si layer on f.s. substrate |
| 15 | Ag STF nanorods | 1.7*, 1.4** | *Ag dense, **Si(100) | Ag nanorods height 170 nm (the first 70 nm is closed) (nominal) 20 nm Si layer Si(100) |
| 16 | Ag STF nanorods | 10*, 5.17** | *Ag dense **f.s. | Ag nanorods height 170 nm (the first 70 nm is closed) without capping layer on f.s. substrate |
| 17 | Ag STF nanorods | 4.5*, 2.3** | *Ag dense, **Si(100) | Ag nanorods height 170 nm (the first 70 nm is closed) (nominal) 10 nm Si layer Si(100) |
| 18 | Ag STF nanorods | 2.7*, 1.065* | *Ag dense, **f.s. | Ag nanorods height 170 nm (the first 70 nm is closed) (nominal) 20 nm Si layer on f.s. substrate |
| 19 | Ag STF nanorods | 71*, 36** | *Ag dense, **Si(100) | $h = 400$ nm, $d = 75$ nm, $\alpha = 23^\circ$, on Si(100) substrate |

Table 1 (Continued).

| # | Sample | Enhancement | Reference | Description |
|----|---------------------------------|----------------|----------------------|---|
| 20 | Si rods on Au dots | 0.8*, 1.52** | *Au dense, **Si(111) | Vertically aligned Si nanorods on hexagonally arranged Au dots, $h(\text{Au}) = 32$ nm (nominal), $h(\text{Si}) = 740$ nm, Substrate: Si(111) |
| 21 | Si rods on Si(100) | 0.71 | Si(111) | Vertically aligned Si nanorods on bare Si(100) $h(\text{Si}) = 740$ nm, Substrate: Si(111) |
| 22 | Au dots, $h(\text{Au}) = 2$ nm | 0.6*, 1.06** | *Au dense, **Si(111) | Si(111) with Au dots in hexagonal arrangement $h(\text{Au}) = 2$ nm |
| 23 | Au dots, $h(\text{Au}) = 46$ nm | 0.75*, 1.336** | *Au dense, **Si(111) | Si(111) with Au dots in hexagonal arrangement $h(\text{Au}) = 46$ nm |

^aThe mean value of the grabbed fluorescence images. *Single or **double asterisks near the enhancement factor values in the column named "Enhancement" relate to the metal or substrate respectively as a reference from column "Reference." Enhancement factor values were calculated according to the Eq. (1).

(Table 1). Note that the enhancement factor can reach from a few 10 s up to 71 in certain cases when measured on hot spots.

Table 1 summarizes the main results of this study, showing a wide spectrum of results, with the most prominent being the fact that Ag STFs result in the greatest fluorescence *e.f.* The parameters used in the table are defined in Fig. 1(b). The Ag-coated Si STF samples resulted in a relatively high *e.f.* as well. The Al nanorods on bare Si substrates exhibited the next level of enhancement. According to Table 1, Au STFs show no enhancement, which is somehow surprising. On the other hand, for the sample containing Si spirals on Au nanodots, an *e.f.* of four was observed. It remains unclear whether the Si or the underlying Au dots (dot size in the range of $d \approx 150$ nm in diameter and an approximate $h = 30$ nm) is responsible for this enhancement; thus this might indicate the importance of the size of the Au nanoparticles in determining the fluorescence enhancement. It might also be possible that sometimes the rods in the metal STFs touch each other, thereby forming broader structures and canceling the nanorod lightening effect. LSPR excitation is not seen from the reflection and transmission spectra that we carried out. Previous work⁵³ showed that this occurs in the mid-infrared range of the spectrum and some were designed specifically for an excitation wavelength of 780 nm, however they show a weak and broad absorption peak.⁵⁴ Porosity is another factor that can enhance fluorescence due to a larger surface-to-volume ratio, which we think did not play a role here because the thin dye film used for this study covers mainly the top surface of the sample. We explored the effect of photo-bleaching and found that reduction of the fluorescence signal is surface-morphology-dependent. For this reason, all of the results presented on Table 1 were measured under the same conditions.

The complex geometries involved in both the silver morphology and the placement of the Rhodamine 123 dye make the results summarized in Table 1 difficult to quantify and evaluate. Most often, comparisons between substrates with and without sculptured or dens silver are made to assess the degree of enhancement. In these instances, the rough silver topology causes dramatic changes in the surface area so that many more emitters can be adsorbed, making it difficult to quantify the enhancement. Also, results tend to be averaged over large numbers of silver nanoparticle aggregates and dye-to-silver separations whose enhancement may be very different. Finally, little effort is generally made to separate contributions of absorption and emissive rate enhancements to the overall increases in fluorescence. According to Table 1, the STF with the highest *e.f.* is Ag columns on Si(100). Since we are also interested in the comparison between the SEF from bacteria on STF^{32,52}—non-specific sensing, and with the immobilized receptors on surfaces—specific sensing, STFs of Ag columns on f.s. (Fig. 4 shows the topology of the structure) were used for the purpose of this study.

Figure 5 shows an example of two fluorescence images, the right side for a Ag STF (thickness approximately 400 nm) deposited by e-beam evaporation on fused silica. The right image consists of a rod-like nanostructure with a rod diameter of $d \approx 75$ nm, inclined at an angle $\alpha \approx 23$ deg with respect to the substrate plane. The left image corresponds to the continuous Ag film

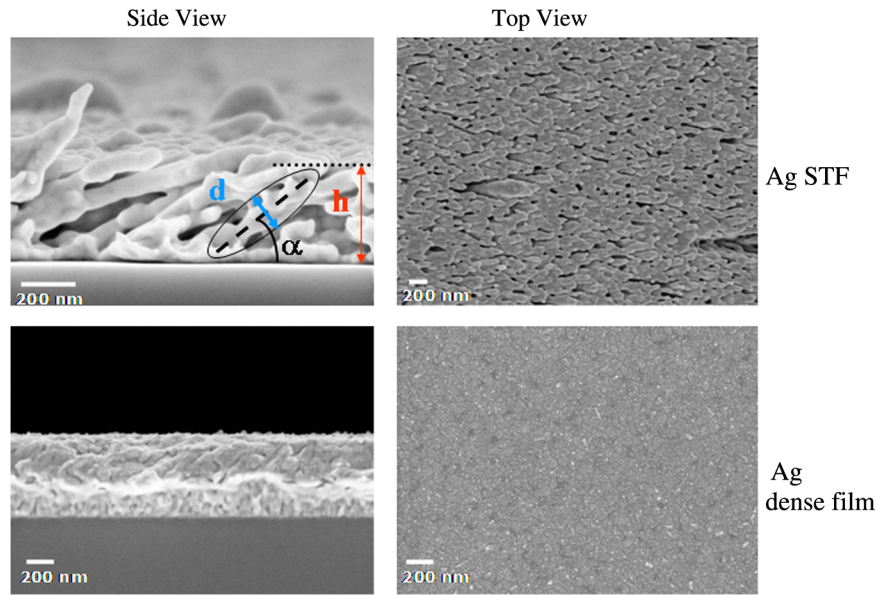


Fig. 4 SEM micrographs of the side (left) and top (right) views of Ag STF (upper) structure that gives highest fluorescence signal enhancement factor with $h \approx 400$ nm, $d \approx 75$ nm, and $\alpha \approx 23$ deg compared to the dens silver film (bottom) with $\alpha \approx 85\text{--}90$ deg.

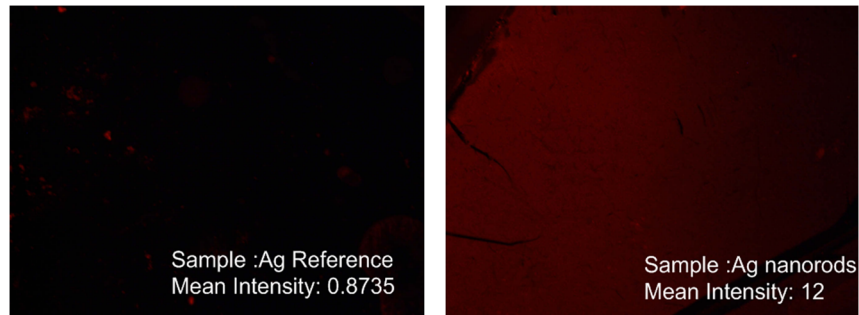


Fig. 5 Example of fluorecence using Rhodamine 123. Images grabbed from closed silver film (left), and columnar silver STF (right).

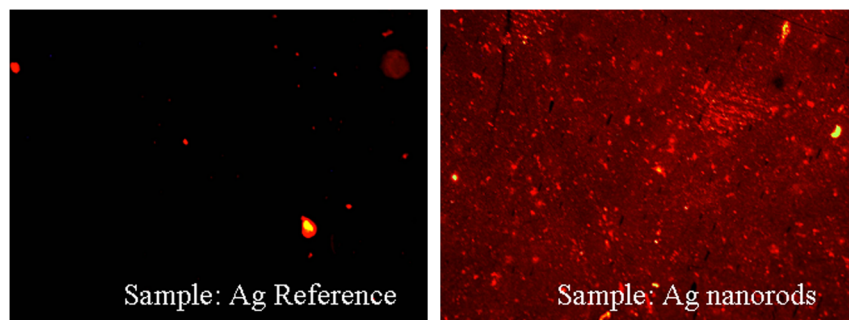


Fig. 6 Fluorecence images for immobilized fluorescent receptor Anti-Rabbit IgG grabbed from closed silver film (left) and columnar silver STF (right).

used as a reference, which has a thickness of approximately 415 nm (deposited on fused silica). Visually one can easily see that the STF enhances the fluorescence signal compared to a closed film. Averaged signal measurements show an enhancement factor of 15.

Figure 6 shows fluorescence images for an immobilized fluorescent receptor Anti-Rabbit IgG (1/100 antibody/PBS) grabbed from closed silver film (left), and columnar silver STF (right), showing an enhancement factor of about 32. The right image consists of a rod-like nanostructure

with rod diameter of $d \approx 75$ nm, inclined at an angle $\alpha \approx 23$ deg with respect to the substrate plane, while the left image corresponds to the flat silver film used as a reference in both samples with approximately 400 nm silver height.

4 Conclusion

SEF from metallic nano-STFs is investigated with a microspot resolution. An extensive comparative study was presented involving experimental results of fluorescent signals from a variety of STFs compared to the reference/dens films using Rhodamine 123 dye as a fluorophore and immobilized fluorescence receptor. Fluorescent signals were captured by a CCD camera, and a specially designed optical fiber housing attached to the microscope allowed quantitative measurements of the fluorescence spectrum on a microspot in parallel with the image grab. A fluorescent enhancement factor of ≈ 20 was obtained from the silver nanocolumns deposited at 23 deg with respect to the f.s. substrate. Enhancement factors from a few 10 s up to 71 were also observed on hot spots. The expected absolute values are much higher than what we reported here. It is believed that this is due to several reasons: (1) There is a distribution of nanorod sizes in the STF, (2) the nanorods are not isolated completely and sometimes clusters of rods touch each other, and (3) some quenching effects can reduce the enhancement. This study highlights the potential of metallic STFs for biosensing. Further studies are needed for: optimizing these structures to specific applications, finding the minimal dimensions of the assay in terms of the detection limit and demonstrating single molecule detection, and lifetime measurements can add to better understanding of the origins of the fluorescence enhancement mechanism near nano-structured metallic nanocolumns and distinguish between the enhanced absorption and the enhanced emission.

Acknowledgments

The authors are grateful to Dr. Christian Patzig and Professor Akhlesh Lakhtakia for the useful discussions during the early stages of this research. Chinmay Khare would like to acknowledge the Graduate school BuildMoNa at University Leipzig in Germany [within the German Excellence Initiative of the Deutsche Forschungsgemeinschaft (DFG)], for its financial support. This work is partially supported by the Singapore National Research Foundation CREATE program “Nanomaterials for Energy and Water Management.”

References

1. T. Hirschfeld, “Quantum efficiency independence of the time integrated emission from a fluorescent molecule,” *Appl. Opt.* **15**(12), 3135–3139 (1976), <http://dx.doi.org/10.1364/AO.15.003135>.
2. C. K. C. Maurice et al., “Controlling optical properties and surface morphology of dry etched porous silicon,” *J. Nanophoton.* **5**(053503), 1–10 (2011), <http://dx.doi.org/10.1117/1.3571270>.
3. M. Babak et al., “Silicon nanophotonic devices for integrated sensing,” *J. Nanophoton.* **3**(031001), 1–23 (2009), <http://dx.doi.org/10.1117/1.3122986>.
4. S. Kalele et al., “Plasmon-assisted photonics at the nanoscale,” *J. Nanophoton.* **1**(012501), 1–20 (2007), <http://dx.doi.org/10.1117/1.2748429>.
5. S. Kuhn et al., “Enhancement of single-molecule fluorescence using a gold nanoparticle as an optical nanoantenna,” *Phys. Rev. Lett.* **97**(017402), 1–4 (2006), <http://dx.doi.org/10.1103/PhysRevLett.97.017402>.
6. A. J. Haes and R. P. Van Duyne, “A unified view of propagating and localized surface plasmon resonance biosensors,” *Anal. Bioanal. Chem.* **379**(7–8), 920–930 (2004), <http://dx.doi.org/10.1007/s00216-004-2708-9>.
7. R. L. Joseph, “Plasmonics in biology and plasmon—controlled fluorescence,” *Plasmonics* **1**(1), 5–33 (2006), <http://dx.doi.org/10.1007/s11468-005-9002-3>.

8. A. Shalabney and I. Abdulhalim, "Sensitivity-enhancement methods for surface plasmon sensors," *Laser Photonics Rev.* **5**(4), 571–606 (2011), <http://dx.doi.org/10.1002/lpor.v5.4>.
9. T. W. Ebbesen et al., "Extraordinary optical transmission through sub-wavelength hole arrays," *Nature* **391**(6668), 667–669 (1998), <http://dx.doi.org/10.1038/35570>.
10. A. Karabchevsky et al., "Theoretical and experimental investigation of enhanced transmission through periodic metal nanoslits for sensing in water environment," *Plasmonics* **4**(4), 281–292 (2009), <http://dx.doi.org/10.1007/s11468-009-9104-4>.
11. E. J. Sanchez, L. Novotny, and X. S. Xie, "Near-field fluorescence microscopy based on two-photon excitation with metal tips," *Phys. Rev. Lett.* **82**(20), 4014–4017 (1999), <http://dx.doi.org/10.1103/PhysRevLett.82.4014>.
12. C. Neacsu, G. Steudle, and M. Raschke, "Plasmonic light scattering from nanoscopic metal tips," *Appl. Phys. B: Lasers Opt.* **80**(3), 295–300 (2005), <http://dx.doi.org/10.1007/s00340-005-1748-y>.
13. C. L. Haynes and R. P. Van Duyne, "Plasmon-sampled surface-enhanced raman excitation spectroscopy," *J. Phys. Chem. B.* **107**(30), 7426–7433 (2003), <http://dx.doi.org/10.1021/jp027749b>.
14. K. Kneipp et al., "Surface-enhanced Raman scattering and biophysics," *J. Phys.: Condens. Matter.* **14**(18), 597–624 (2002), <http://dx.doi.org/10.1088/0953-8984/14/18/202>.
15. A. M. Michaels, M. Nirmal, and L. E. Brus, "Surface enhanced raman spectroscopy of individual rhodamine 6g molecules on large Ag nanocrystals," *J. Am. Chem. Soc.* **121**(43), 9932–9939 (1999), <http://dx.doi.org/10.1021/ja992128q>.
16. S. Nie and S. R. Emory, "Probing single molecules and single nanoparticles by surface-enhanced raman scattering," *Science* **275**(5303), 1102–1106 (1997), <http://dx.doi.org/10.1126/science.275.5303.1102>.
17. E. A. Wachter, A. K. Moore, and J. W. Haas III, "Fabrication of tailored needle substrates for surface-enhanced Raman scattering," *Vib. Spectros.* **3**(1), 73–78 (1992), [http://dx.doi.org/10.1016/0924-2031\(92\)85026-W](http://dx.doi.org/10.1016/0924-2031(92)85026-W).
18. J. L. Martínez, Y. Gao, and T. López-Ríos, "Surface-enhanced Raman scattering of obliquely evaporated Ag films," *Phys. Rev. B* **33**(8), 5917–5919 (1986), <http://dx.doi.org/10.1103/PhysRevB.33.5917>.
19. J. Vuckovic, M. Loncar, and A. Scherer, "Surface plasmon enhanced light-emitting diode," *IEEE J. Quantum Electron.* **36**(10), 1131–1144 (2000), <http://dx.doi.org/10.1109/3.880653>.
20. P. A. Hobson et al., "Surface plasmon mediated emission from organic light-emitting diodes," *Adv. Mater.* **14**(19), 1393–1396 (2002), [http://dx.doi.org/10.1002/1521-4095\(20021002\)14:19<1393::AID-ADMA1393>3.0.CO;2-B](http://dx.doi.org/10.1002/1521-4095(20021002)14:19<1393::AID-ADMA1393>3.0.CO;2-B).
21. J. R. Lakowicz, "Radiative decay engineering: biophysical and biomedical applications," *Anal. Biochem.* **298**(1), 1–24 (2001), <http://dx.doi.org/10.1006/abio.2001.5377>.
22. R. R. Chance, A. Prock, and R. Silbey, *Molecular Fluorescence and Energy Transfer Near Interfaces*, Wiley, New Jersey (2007).
23. W. L. Barnes, "Fluorescence near interfaces: the role of photonic mode density," *J. Mod. Opt.* **45**(4), 661–699 (1998), <http://dx.doi.org/10.1080/09500349808230614>.
24. E. Dulkeith et al., "Fluorescence quenching of dye molecules near gold nanoparticles: radiative and nonradiative effects," *Phys. Rev. Lett.* **89**(20), 1–4 (2002), <http://dx.doi.org/10.1103/PhysRevLett.89.203002>.
25. E. Dulkeith et al., "Gold nanoparticles quench fluorescence by phase induced radiative rate suppression," *Nano Lett.* **5**(4), 585–589 (2005), <http://dx.doi.org/10.1021/nl0480969>.
26. F. Cannone et al., "Quenching and blinking of fluorescence of a single dye molecule bound to gold nanoparticles," *J. Phys. Chem. B.* **110**(33), 16491–16498 (2006), <http://dx.doi.org/10.1021/jp0625816>.
27. S. Pan, Z. Wang, and L. J. Rothberg, "Enhancement of adsorbed dye monolayer fluorescence by a silver nanoparticle overlayer," *J. Phys. Chem. B.* **110**(35), 17383–17387 (2006), <http://dx.doi.org/10.1021/jp063191m>.
28. O. Kulakovich et al., "Enhanced luminescence of cdse quantum dots on gold colloids," *Nano Lett.* **2**(12), 1449–1452 (2002), <http://dx.doi.org/10.1021/nl025819k>.

29. K. Sokolov, G. Chumanov, and T. M. Cotton, "Enhancement of molecular fluorescence near the surface of colloidal metal films," *Anal. Chem.* **70**(18), 3898–3905 (1998), <http://dx.doi.org/10.1021/ac9712310>.
30. F. Xie, M. S. Baker, and E. M. Goldys, "Homogeneous silver-coated nanoparticle substrates for enhanced fluorescence detection," *J. Phys. Chem. B* **110**(46), 23085–23091 (2006), <http://dx.doi.org/10.1021/jp062170p>.
31. P. Anger, P. Bharadwaj, and L. Novotny, "Enhancement and quenching of single-molecule fluorescence," *Phys. Rev. Lett.* **96**(11), 1–4 (2006), <http://dx.doi.org/10.1103/PhysRevLett.96.113002>.
32. I. Abdulhalim et al., "Surface-enhanced fluorescence from metal sculptured thin films with application to biosensing in water," *Appl. Phys. Lett.* **94**(063106), 1–3 (2009), <http://dx.doi.org/10.1063/1.3081031>.
33. P. C. Das and A. Puri, "Energy flow and fluorescence near a small metal particle," *Phys. Rev. B* **65**(155416), 1–8 (2002), <http://dx.doi.org/10.1103/PhysRevB.65.155416>.
34. O. Andreussi et al., "Radiative and nonradiative decay rates of a molecule close to a metal particle of complex shape," *J. Chem. Phys.* **121**(20), 10190–10202 (2004), <http://dx.doi.org/10.1063/1.1806819>.
35. A. Lakhtakia and R. Messier, *Sculptured Thin Films: Nanoengineered Morphology and Optics*, SPIE, Bellingham (2005).
36. K. Robbie, M. J. Brett, and A. Lakhtakia, "First thin film realization of a helicoidal bianisotropic medium," *J. Vac. Sci. Technol. A* **13**(6), 2991–2993 (2009), <http://dx.doi.org/10.1116/1.579626>.
37. I. J. Hodgkinson et al., "Spacerless circular-polarization spectral-hole filters using chiral sculptured thin films: theory and experiment," *Opt. Commun.* **184**(1–4), 57–66 (2000), [http://dx.doi.org/10.1016/S0030-4018\(00\)00935-4](http://dx.doi.org/10.1016/S0030-4018(00)00935-4).
38. A. C. van Popta et al., "Gradient-index narrow-bandpass filter fabricated with oblique-angle deposition," *Opt. Lett.* **29**(21), 2545–2547 (2004), <http://dx.doi.org/10.1364/OL.29.002545>.
39. A. Shalabney et al., "Sensitivity of surface plasmon resonance sensors based on metallic columnar thin films in the spectral and angular interrogations," *Sens. Actuators, B* **159**(1), 201–212 (2011), <http://dx.doi.org/10.1016/j.snb.2011.06.072>.
40. M. Motyka and A. Lakhtakia, "Multiple trains of same-color surface plasmon-polaritons guided by the planar interface of a metal and a sculptured nematic thin film. Part IV Canonical problem," *J. Nanophoton.* **4**(043505), 1–3 (2008), <http://dx.doi.org/10.1117/1.3033757>.
41. M. Motyka and A. Lakhtakia, "Multiple trains of same-color surface plasmon-polaritons guided by the planar interface of a metal and a sculptured nematic thin film. Part II: arbitrary incidence," *J. Nanophotonics* **3**(033502), 1–13 (2009), <http://dx.doi.org/10.1117/1.3147876>.
42. I. Abdulhalim, "Nanophotonic and subwavelength structures for sensing and biosensing," in *Springer Series on Chemical Sensors and Biosensors*, Springer, Berlin Heidelberg, 73–106 (2010).
43. E. Goldys et al., "Plasmon-enhanced fluorescence near metallic nanostructures: biochemical applications," *Appl. Phys. A: Mater. Sci. Process.* **89**(2), 265–271 (2007), <http://dx.doi.org/10.1007/s00339-007-4100-z>.
44. R. Luchowski et al., "Plasmonic platforms of self-assembled silver nanostructures in application to fluorescence," *J. Nanophoton.* **4**(043516), 1–17 (2010), <http://dx.doi.org/10.1117/1.3500463>.
45. R. Messier and A. Lakhtakia, "Sculptured thin films—II. Experiments and applications," *Mater. Res. Innovations.* **2**(4), 217–222 (1999), <http://dx.doi.org/10.1007/s100190050088>.
46. C. Patzig et al., "Silicon nanocolumns on nanosphere lithography templated substrates: effects of sphere size and substrate temperature," *J. Nanosci. Nanotechnol.* **9**(6), 1985–1991 (2009), <http://dx.doi.org/10.1166/jnn.2009.367>.
47. B. Fuhrmann et al. "Ordered arrays of silicon nanowires produced by nanosphere lithography and molecular beam epitaxy," *Nano Lett.* **5**(12), 2524–2527 (2005), <http://dx.doi.org/10.1021/nl051856a>.

48. C. Patzig and B. Rauschenbach, "Temperature effect on the oblique angle deposition of Si sculptured thin films," in *54th International AVS Symp.*, Seattle, Washington, pp. 881–886 (2008).
49. C. Khare et al., "Influence of substrate temperature on oblique angle deposited Ag nanorods," *J. Vac. Sci. Technol. A* **28**(4), 1002–1009 (2010).
50. C. Patzig et al., "Periodically arranged Si nanostructures by oblique angle deposition on patterned substrates," *Phys. Status Solidi* **247**(6), 1322–1334 (2010), <http://dx.doi.org/10.1002/pssb.v247:6>.
51. D. B. Murphy, *Fundamentals of Light Microscopy and Electronic Imaging*, Wiley, New York (2001).
52. I. Abdulhalim et al., "Comparative study of enhanced fluorescence from nano sculptured thin films," *Proc. SPIE* **7041**, 70410G (2008), <http://dx.doi.org/10.1117/12.795139>
53. A. I. Maarof et al., "Bulk and surface plasmons in highly nanoporous gold films," *J. Phys. D: Appl. Phys.* **40**(18), 5675–5682 (2007), <http://dx.doi.org/10.1088/0022-3727/40/18/024>.
54. M. Suzuki et al., "In-line aligned and bottom-up Ag nanorods for surface-enhanced Raman spectroscopy," *Appl. Phys. Lett.* **88**(20), 1–3 (2006), <http://dx.doi.org/10.1063/1.2205149>.



Alina Karabchevsky received her BS and MS in biomedical engineering from the Ben-Gurion University of the Negev, Beer-Sheva, Israel in 2005 and 2008 respectively. During her master degree studies she specialized on biomedical signal processing. Recently, she submitted her PhD dissertation in electro-optics engineering to Ben Gurion University. Her research interests were plasmonic nano-structures and optical biosensing devices, combining her biomedical engineering background with optics and physics.



Chinmay Khare obtained his PhD in physics from the 'BuildMoNa' graduate school, Universität Leipzig under supervision of professor Dr. B. Rauschenbach at Leibniz Institute of Surface Modification, Leipzig. His research interests focus on synthesis and characterization of glancing angle deposited nanostructures. In January 2012 he became a post-doc at Ruhr-Universität Bochum, Germany.



Bernd Rauschenbach is the director of the Leibniz Institute of Surface Modification (IOM) and professor of applied physics at the University Leipzig (Germany). His fields of research are the interaction of ion and laser beams with solid surfaces, the nanotechnology, and the preparation and characterization of thin films.



Ibrahim Abdulhalim is a professor and head of the Department of Electrooptic Engineering at Ben Gurion University. He has worked in academic institutions and companies such as the OCSC in UC at Boulder, the ORC at Southampton University, the Thin Films Center of the University of Western Scotland, in KLA-Tencor, Nova and GWS Photonics. His current research involve: LC devices, nanophotonics for biosensing, biomedical optical imaging techniques. He has published over 160 articles, one book, and 10 patents. He is a Fellow of IoP and SPIE and an associate editor for the *Journal of Nanophotonics* and for the *Journal of Physics Express*.